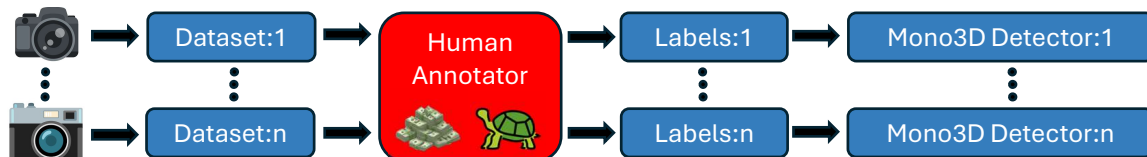


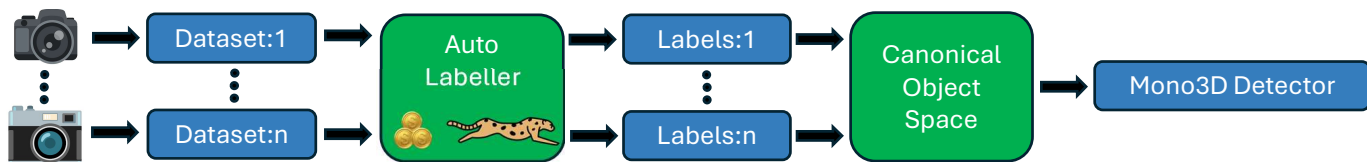
MonoSOWA: Scalable monocular 3D Object detector Without human Annotations

Jan Skvrna
Dept. of Cybernetics
FEE, Czech Technical University
skvrnjan@fel.cvut.cz

Lukas Neumann
Dept. of Cybernetics
FEE, Czech Technical University
lukas.neumann@cvut.cz



(a) Traditional pipelines require human labelling and produce new model for every different camera setup



(b) Our method does not need human labelling and combines multiple camera setups into a single model operating in canonical object space

Fig. 1: Traditional pipelines (a) vs. the proposed pipeline (b) for monocular 3D object detection.

Abstract—Detecting the three-dimensional position and orientation of objects using a single RGB camera is a foundational task in computer vision with many important applications. Traditionally, 3D object detection methods are trained in a fully-supervised setup, requiring vast amounts of human annotations, which are laborious, costly, and do not scale well with the ever-increasing amounts of data being captured.

In this paper, we present the first method to train 3D object detectors for monocular RGB cameras without domain-specific human annotations, thus making orders of magnitude more data available for training. Thanks to newly proposed Canonical Object Space, the method can not only exploit data across a variety of datasets and camera setups to train a single 3D detector, but unlike previous work it also works out of the box in previously unseen camera setups. All this is crucial for practical applications, where the data and cameras are extremely heterogeneous.

The method is evaluated on two standard autonomous driving datasets, where it outperforms previous works, which, unlike our method, still rely on 2D human annotations. The source code and the model is going to be published soon.

I. INTRODUCTION

Monocular 3D object detection is a key component of many important systems, ranging from robotics to autonomous cars. 3D object detection methods are typically trained in a fully-supervised setup, requiring vast amounts of human annotations, which are laborious, costly, and do not scale well with ever-increasing amounts of data that ideally should be used for training. To make matters even worse, especially in autonomous driving, new cameras and new camera setups

emerge constantly, which typically implies the need to collect, label and train on a new dataset as camera parameters such as focal length change.

In this paper, we address both of these challenges – costly human labels and changing camera setup – by introducing a new method to *train a 3D rigid object detector in a Canonical Object Space without domain-specific human labels*. Our method allows us to exploit large amounts of training data readily available because all we need as input for training are unlabelled driving video sequences. Furthermore, our method does not require data from additional sensors such as LiDAR. It makes our method extremely applicable in practice because as such our method can directly exploit data collected by a majority of currently manufactured vehicles, which typically only have a single camera. This is in contrast with some methods which require LiDAR (and human annotations) [1], [2], because for them specialised vehicles are needed to collect the data, and this severely limits the variety of geographies, environments, and traffic situations being captured.

Drawing inspiration from monocular depth literature [3], the proposed Canonical Object Space (COS) allows us to aggregate and learn from data coming from different cameras, which is a crucial pre-condition to being able to effectively harvest otherwise very heterogeneous video sequences. Moreover, unlike previous methods such as VSRD [4], it also allows for the deployment of our 3D object detector in new unseen camera setup *without needing to train or fine-tune for the new setup*. This is again extremely useful in practice, because new

camera sensors and setups are developed all the time, but it is unfeasible to collect data, label them by human annotators, and then train a new model for each new camera type.

To summarize, we make the following contributions:

- 1) We propose a novel auto-labelling pipeline which exploits temporal consistency in video sequences to automatically generate 3D position, size, and orientation labels of rigid objects (cars) from a monocular camera.
- 2) To the best of our knowledge, our method is the first method to train a monocular 3D object detector for autonomous driving which *does not require neither 2D nor 3D human annotations*; we demonstrate to the community that such an approach is feasible and is worth pursuing further.
- 3) We propose novel Canonical Object Space (COS), which allows us to a) aggregate data from different camera setups in training, and b) at inference time, use an already trained model in the previously unseen camera setup, i.e. without any training or fine-tuning for the new setup.
- 4) Our auto-labelling method is significantly faster than previous work, allowing us to process significantly more training data than the current state-of-the-art method.

II. RELATED WORK

a) Monocular Depth Estimation: Monocular depth estimation has shown significant improvements in recent years. MiDAS [5] employs affine-invariant losses to enable training on multiple datasets. ZoeDepth [6] combines training on multiple datasets with relative losses and further fine-tunes on the target metric dataset. Depth Anything [7] focuses on the affine-invariant depth estimation using self-supervised pre-training. For metric depth estimation, which is relevant for object detection, it fine-tunes on the target dataset such as KITTI [8]. Metric3D [3], [9] focuses on **metric** depth estimation as it uses a Canonical Camera Transformation Module to further improve zero-shot performance, together with DINOv2 [10] or ConvNext [11] as the backbone and DPT [12] as the predictor. CamConv [13] models cameras inside the network, but as shown in [3], this leads to poor results.

b) Fully-supervised Monocular 3D Object Detection:

Early methods [14]–[16] were based on lifting the image into pseudo-LiDAR and then detecting objects in the generated point cloud. SMOKE [17], on the other hand, directly predicts 3D bounding boxes from images. MonoDTR [18] and MonoDETR [19] use an end-to-end depth-aware/guided transformer [20] architecture to directly predict 3D bounding boxes. SSD-MonoDETR [21] introduces scale awareness into the model. MonoATT [22] variably assigns tokens to areas of higher importance. MonoFlex [23] uses an ensemble of direct depth and keypoint-based predictions and decouples the detection of truncated and untruncated vehicles. MonoCD [24] enhances the ensemble with a complementary depth predictor. However, all the aforementioned methods require 3D human annotations during their training.

c) Weakly-supervised 3D Object Detection: Most previous works on weakly-supervised 3D detection have focused on training 3D detectors for LiDAR. VS3D [25] pioneered in this area by using point density in LiDAR scans to identify objects, and detections are further refined by a student-teacher network, where the teacher is trained on images only. Zakharov et al. [2] employs a 2D off-the-shelf detector accompanied by a novel Signed Distance Fields (SDF)-renderer within the DeepSDF framework [26] and Normalized Object Coordinate Space (NOCS). The method is trained on a synthetic dataset and further fine-tuned on real datasets.

WS3D [27], [28] employs Bird’s Eye View (BEV) human-centered clicks as weak supervision to train a network for detecting vehicles, arguing that these are much easier to obtain than 3D bounding boxes. Furthermore, they use a small subset of human ground-truth annotations to train a second network to predict the spatial dimensions of the detected vehicles. McCraith et al. [29] employ direct fitting of generic templates into LiDAR scans segmented by Mask-RCNN [30] and share the information between frames by requiring consistency between frames while simultaneously discounting outliers. TCC-det [31] uses direct fitting of generic templates on aggregated points corresponding to each instance. During the training of the 3D detector, TCC-det appends two additional losses for finer alignment. VG-W3D [32] encodes the image and LiDAR scan separately and then enforces alignment between 2D and 3D on multiple feature levels to predict precise 3D bounding boxes. In contrast to the aforementioned methods, VSRD [4] focuses on 3D detection in camera, and *does not require LiDAR scans*. However, it uses 2D human ground-truth masks for each instance, representing them as a surface in Signed Distance Fields (SDF). Furthermore, the SDF are rendered into masks through their proposed volumetric-aware silhouette rendering, enabling end-to-end training. Each instance is optimized over multiple frames. While VSRD shows promising results in both weakly-supervised and semi-supervised training, it requires 2D instance masks, and rendering of each frame takes approximately 15 minutes. In contrast, our method **does not require any human annotations at all** and is approximately 100 times faster.

III. METHOD

Traditionally, deep networks that predict 3D bounding boxes of vehicles (and other agents) from a single image are trained using 3D annotations, which are manually created by human annotators. They typically rely on both camera image and LiDAR data for correct distance estimate in creating their labels. However, this process is very laborious and costly, limiting the amount of training data available to train such methods. Moreover, it requires capturing the scene using both a camera and a LiDAR sensor, which is a significant limitation since the majority of production vehicles these days do not have LiDAR on board – as a result, data collection is only limited to vehicles dedicated to such a purpose, and this again limits the variety and diversity of data being used to train these methods.

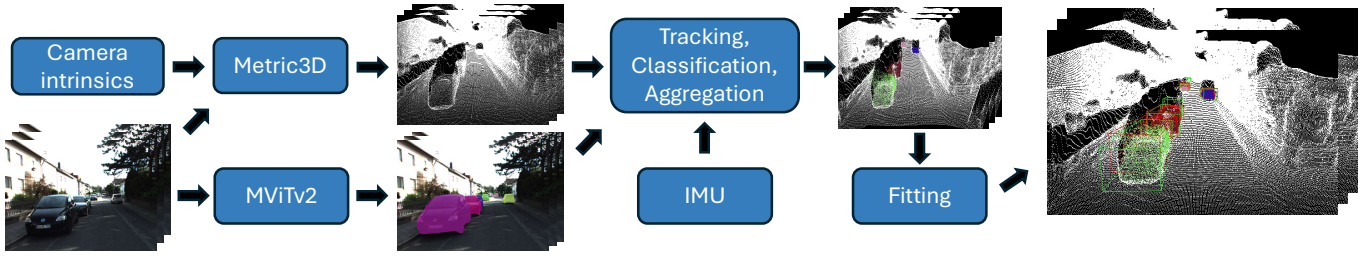


Fig. 2: Our auto-labelling pipeline creates 3D pseudo-groundtruth using only images, camera parameters and IMU data as inputs.

Our method overcomes these limitations by introducing a novel approach to train a 3D object detector using only images (and vehicle motion data) as inputs, without requiring *human labels* or *LiDAR* in the training process.

A. Auto-labelling pipeline

The process of automatic label creation assumes that images are captured in a sequence, which is a natural way to capture data in driving scenarios. It also assumes that the camera setup is known (both intrinsics and extrinsics) for each sequence. However, the camera setup might be and actually often is different (see section III-B). Lastly, it assumes approximate data about ego-vehicle’s motion is available (e.g. from GPS or an Inertial Measurement Unit – IMU), which again is commonplace.

Because labelling a 7-DOF pose of objects jointly is a very challenging problem, we instead infer individual pose parameters separately in a sequence of steps.

a) Detecting objects in pseudo-LiDAR: The auto-labelling process begins by inferring a metric depth map $D \in \mathbb{R}^{h \times w}$ for each camera image $I \in \mathbb{R}^{3 \times h \times w}$, where h and w denotes image height and width, using an off-the-shelf monocular depth estimator. We opted to use Metric3D [3], as it is zero-shot, it does not limit our method in terms of data distribution and has shown great results for generalization. The choice of a particular monocular metric depth estimator is, however, not crucial. For each pixel and its corresponding depth, a 3D point cloud is generated as

$$\begin{aligned} X_{u,v} &= \frac{D_{u,v} \cdot (u - c_x)}{f_x} \\ Y_{u,v} &= \frac{D_{u,v} \cdot (v - c_y)}{f_y} \\ Z_{u,v} &= D_{u,v} \end{aligned} \quad (1)$$

where $u \in [0, h]$ and $v \in [0, w]$, c is the principal point and f is the focal length. We denote the pseudo lidar point cloud as $P_i \in \mathbb{R}^{3 \times h \times w}$, where i stands for the frame index.

Next, inspired by [29], we employ an off-the-shelf 2D object image detector to detect the objects we are interested in (vehicles) and their instance segmentation masks in each camera image. Given an instance segmentation mask $M_{i,j} \in \mathbb{R}^{h \times w}$

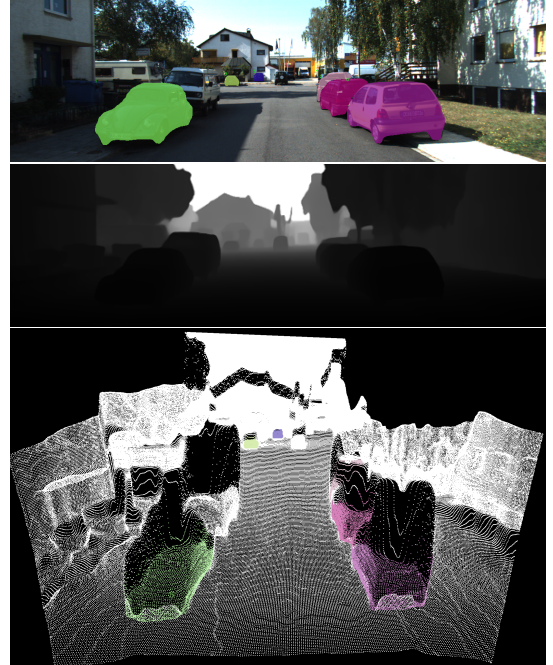


Fig. 3: Combining instance segmentation in image (top) with monocular metric depth estimation (middle) enables us to produce pseudo-LiDAR point cloud for each object.

of an object j in a frame i , we find object point cloud $P_{i,j}$ in the point cloud as

$$P_{i,j} = \{p \in P_i \mid \mathcal{T}(p) \in M_{i,j}\} \quad (2)$$

where $\mathcal{T}(p)$ denotes the projection of the 3D point p into image coordinates (using camera calibration, which is known).

The $P_{i,j}$ tends to contain outliers, as either the masks or the metric depth estimation is not perfect. To remove the outliers, an ensemble of the following methods is employed: HBOS [33], Z-scores, statistical outlier rejection in Open3D [34], HDBSCAN [35] and DBSCAN [36]. If at least two of these methods classify a point as an outlier, it is removed. To compensate for the effect of the ego-vehicle movement, we transform all $P_{i,j}$ into the reference frame coordinate space, given the poses from IMU data.

b) Temporal consistency: In order to exploit temporal consistency across multiple frames of the sequence, we need to first establish correspondences of individual object instances between frames. Because we have inferred approximate 3D point cloud of each object instance $P_{i,j}$ in each frame, we track each object in 3D world coordinate system.

For each object j in frame i , we approximate its location $L_{i,j}$ as the median of its point cloud $P_{i,j}$. The tracking is initialized in n frames before the reference (current) frame, and for each frame, it matches the instances based on locations in the current frame $L_{i,j}$ and the predicted future locations from the last frame into the current frame $\hat{L}_{i,j}$. For the location prediction $\hat{L}_{i,j}$, a simple physics-aware motion model is used

$$\hat{L}_{i,j} = L_{i-1,j} + \frac{1}{3} \sum_{k=1}^3 L_{i-k,j} - L_{i-k-1,j} \quad (3)$$

To match two object instances between frames, it is required that the instances are both their nearest neighbours and that the distance between them is lower than a set threshold T_{dist} . Otherwise, the instance is considered as a new object. After this step, each object instance is represented by extracted points $P_{i,j}$ and locations $L_{i,j}$ in each frame the instance is present. The tracking sequentially processes all the frames up to n after the reference frame.

c) Movement Classification: The next step is to classify instances as either stationary or moving, as different principles of temporal consistency exploitation are applied to those classes. Note that all object instances actually appear moving – they change location in relative terms, as the ego-vehicle itself is driving while data is captured.

In order to classify a vehicle as stationary or moving, we propose the following novel classification procedure. For each instance, all locations $L_{m\dots n,j}$ are taken and differences between all adjacent locations are computed, where m is the first frame, where the instance is present and n is the last. From those differences, the standard deviation σ is calculated as

$$\sigma_j = \frac{1}{\sqrt{2}} \sqrt{\frac{1}{n-m} \sum_{i=m+1}^n (\mu_j - D_{i,j})^2} \quad (4)$$

$$\mu_j = \frac{1}{n-m} \sum_{i=m+1}^n D_{i,j} \quad D_{i,j} = L_{i,j} - L_{i-1,j} \quad (5)$$

Furthermore, the actual distance d and expected distance \hat{d} caused by the σ is calculated as

$$d_j = \|L_{m,j} - L_{n,j}\|_2^2 \quad \hat{d}_j = (n-m) \cdot \|\sigma_j\|_2^2 \quad (6)$$

The z - and p -scores are calculated to know if the difference between the d_{real} and d_{exp} is statistically significant or not

$$z_j = \frac{d_j}{\hat{d}_j} \quad p_j = 1 - \Phi(z_j) \quad (7)$$

To classify the instance as moving, the p -score is required to be lower than the threshold T_m and simultaneously, the d

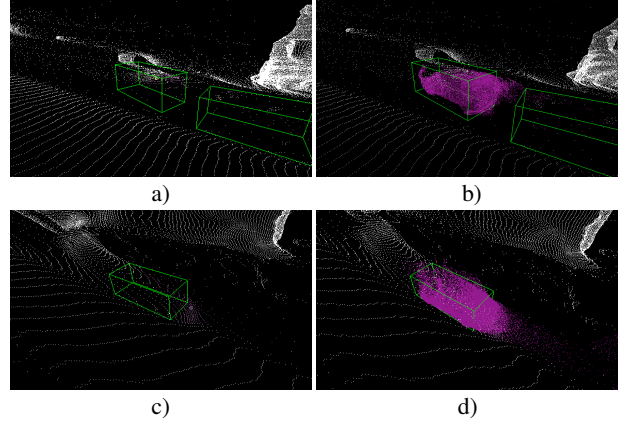


Fig. 4: Temporal aggregation examples. The point cloud of a significantly occluded vehicle (a) is recovered in subsequent frames (b) where the vehicle is no longer occluded. Distant car with poor depth prediction (c) is refined as the ego-vehicle drives closer (d). White points is pseudo-LiDAR of each frame, colourful points are the aggregated points. Human ground truth overlaid as green boxes for reference purposes.

distance must be higher than a given threshold.

As all $P_{i,j}$ are in the reference frame, we can aggregate points for stationary instances by simply concatenating the points

$$A_j = \bigcup_{i=m}^n P_{i,j} \quad (8)$$

Aggregating points for moving instances poses a significant challenge, as the $P_{i,j}$ differs significantly between frames. For that reason, for moving instances, only the trajectory and $P_{i,j}$ are employed.

d) Orientation and size estimation: Finding oriented 3D bounding boxes is a 7-degrees of freedom (DOF) problem. Instead of solving it directly, our method divides it into three disjunctive problems: orientation, location and dimensions.

Orientation estimation is different for moving and stationary instances. For moving instances, the yaw of the object is estimated by directly computing the angle between adjacent locations as

$$\theta_{i,j} = \text{atan2} \left(\frac{L_{i,j}(z) - L_{i-1,j}(z)}{L_{i,j}(x) - L_{i-1,j}(x)} \right) \quad (9)$$

It is worth noting again that all locations are transformed into the reference coordinate space. To make it more robust, yaws for up to 5 locations before and after the reference frame are predicted, and then the median is taken out of those yaw predictions.

For stationary instances, we adapt the 3D box fitting algorithm of Zhang et al. [37]. The algorithm first flattens all points into BEV, and then it iterates over all possible angles $\theta \in 0, \frac{\pi}{2}$. For each angle, two perpendicular axes to each other are computed, and all points are projected into both axes C_1 and C_2 . Further, the criterion is computed, and θ with the minimal loss is chosen.

We propose a novel Saturated Closeness Criterion (algorithm 1). Instead of taking a simple sum of distances d , as Closeness Criterion in Zhang et al. [37], we feed the d into a sigmoid multiplied by steepness parameter α (eq. (10)), inspired by Template Fitting Loss in [31], to saturate the distance of outliers and reduce their influence on the fitting. As a result, the robustness and accuracy of estimation in noisy point clouds are significantly improved over the original algorithm.

$$d = \sigma(\alpha \cdot d) \quad (10)$$

Another modification is that Closeness Criterion computes the distance to either minimum or maximum. However, those extremal points tend to be outliers. To mitigate the problem, each point is assigned either to the 10th or 90th percentile of the projected points instead of min/max. Intuitively, this creates an axis at the most probable location, mitigating outliers' influence.

Algorithm 1 Saturated Closeness Criterion

Require: k ▷ Steepness parameter

- 1: **function** SATURATEDCLOSENESS(C_1, C_2)
- 2: $c_1^{\max} \leftarrow P_{90}(C_1), c_1^{\min} \leftarrow P_{10}(C_1)$ ▷ P is percentile
- 3: $c_2^{\max} \leftarrow P_{90}(C_2), c_2^{\min} \leftarrow P_{10}(C_2)$
- 4: $D_1 \leftarrow \arg \min_{v \in \{c_1^{\max} - C_1, C_1 - c_1^{\min}\}} \|v\|_2$
- 5: $D_2 \leftarrow \arg \min_{v \in \{c_2^{\max} - C_2, C_2 - c_2^{\min}\}} \|v\|_2$
- 6: $D_1 \leftarrow \sigma(\alpha \cdot D_1)$ ▷ σ is the sigmoid function
- 7: $D_2 \leftarrow \sigma(\alpha \cdot D_2)$
- 8: $L \leftarrow 0$
- 9: **for** $i = 1$ to $\text{length}(D_1)$ **do**
- 10: $d \leftarrow \min(D_1(i), D_2(i))$
- 11: $L \leftarrow L + d$
- 12: **end for**
- 13: **return** L
- 14: **end function**

As mentioned, the algorithm chooses the yaw with a minimal loss. It creates two hypotheses, as it doesn't differentiate between the front and back of the car. It is worth noting that the novel Saturated Closeness Criterion does not significantly increase the computational requirements.

To make the estimation more robust, we take both the A_j and multiple $P_{i,j}$. Our method chooses frames so the object instance is the closest possible to the ego-vehicle, but at the same time, it is still fully in view to benefit from the fact that the pseudo-lidar is the most accurate for close predictions.

The algorithm outputs a single spatial dimension for a single frame. If any of the values exceed the expected dimensions of an instance, the output is replaced by a prior estimate of the dimensions of a generic instance. Also, it is necessary to take into account that estimating the spatial dimensions of an instance from a single image can be an ill-posed problem; for example, if an instance is seen from the back, it is not possible to estimate length correctly. Thus, such cases are detected, and again, the output is replaced by a prior car dimensions estimate.

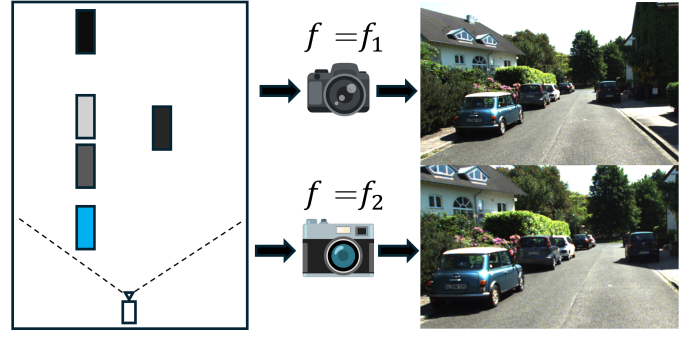


Fig. 5: Inherent ambiguity caused by different camera focal length. The same scene (left) captured by two cameras with different focal length (middle) results in two images (right) where the object has different size. A monocular 3D object detector is however expected to predict the same 3D object location for both images, which is *impossible* without the detector knowing the focal length as well.

e) Position refinement: The yaw $\theta_{i,j}$ and an approximate 3D position $L_{i,j}$ are already known from the previous steps. In order to get a more fine-grained estimate of position $L_{i,j}$, we apply small perturbations (up to 2 meters) along x and z axes and use Template Fitting Loss (TFL) [31] as the criterion to select the final position. In this stage, we also determine whether the car is facing towards or away from the ego-vehicle by testing two hypotheses for vehicle orientation $-\theta$ and $\theta + \pi$ and again selecting the orientation with the lowest TFL. As the orientation, location and dimensions are known at this step, 3D pseudo labels are created and further used to train the Monocular 3D Detector.

B. Canonical Object Space (COS)

Camera focal length is a crucial parameter for precise **metric** depth estimation, but monocular 3D detectors, however, have no direct way to compensate for changing focal length because the same object at the same distance from the camera will have different size in the image, depending on the focal length (see fig. 5).

Assuming an object of size S^{real} with a distance D from the camera in world coordinates, the apparent size (\approx number of pixels) in the image S^{img} is given as

$$\frac{S^{\text{real}} \cdot f_1}{D} = S_1^{\text{img}} \neq S_2^{\text{img}} = \frac{S^{\text{real}} \cdot f_2}{D} \quad (11)$$

where f_1 and f_2 denote the focal length of camera *capturing the same scene*.

Taken to the extreme, for the exact same object image (same size S^{img}), the network needs to predict arbitrarily different distances in world coordinates due to the focal length change. This is clearly impossible, and this phenomenon confuses the network both in training as well as at inference time. When combining multiple datasets that were not taken with a single camera or even a single dataset that used different cameras

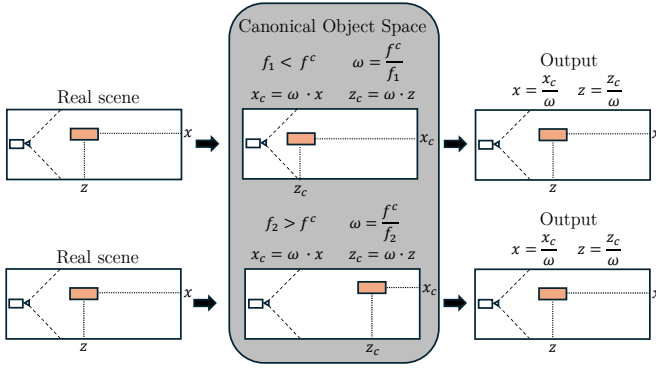


Fig. 6: Canonical Object Space. One scene viewed with two different cameras with different parameters. As the imaging size of the same object is different, 3D labels are scaled accordingly to adapt for focal length change. The predictions and loss computations are all calculated in the Canonical Object Space, and the final predictions are obtained after scaling back based on (known) camera parameters.

to capture the dataset [38], it is a pre-requisite to be able to accommodate focal length differences.

Inspired by Metric3D [3] where depth maps are normalized into a uniform space, our method presents Canonical Object Space (COS) where 3D bounding boxes are trained to be invariant to changes in the focal length by choosing a single canonical focal length and then transforming the labels (objects) into COS. Instead of transforming whole images or depth maps, as in Metric3D, only the x, y, z coordinates of all pseudo-ground truth labels are transformed. To transform labels, the scaling parameter ω_i is calculated as

$$\omega_i = \frac{f^C}{f_i} \quad (12)$$

where f_i stands for the focal length of the frame i and f^C is the canonical focal length. Given the scaling parameter ω_i , the object instance (x, y, z) is transformed into COS as

$$x^C = x \cdot \omega_i \quad y^C = y \cdot \omega_i \quad z^C = z \cdot \omega_i \quad (13)$$

The model then operates in the COS and is directly supervised by the transformed labels (objects). During inference, all predictions are transformed from COS by dividing the depth prediction by scaling parameter ω_j of the inference frame j

$$x = \frac{x^C}{\omega_j} \quad y = \frac{y^C}{\omega_j} \quad z = \frac{z^C}{\omega_j} \quad (14)$$

This very simple transformation enables the network to train on multiple datasets where focal length differs and also allows the network to *work in unseen camera setup* (focal length) because ω_j is calculated at inference time (see table III – 0% fine-tuning row).

Note that in the training process, it is necessary to adapt for data augmentations that affect the perceived focal length of the image, such as image scaling, and for the fact that

the detector resizes the image into a constant input size by adjusting the perceived focal length of the image subject to the applied augmentations and the resizing.

IV. EXPERIMENTS

a) Datasets: We use two public datasets for the evaluation – KITTI [8] and KITTI-360 [39]. KITTI dataset setup has four front-facing cameras, IMU and LiDAR. KITTI-360 setup uses two front-facing cameras and two fish-eye cameras facing sides, IMU and LiDAR. The cameras and their parameters differ in both datasets. For the KITTI dataset, the same training (3712 samples) and validation (3769 samples) splits as [2, [29], [31], [40] are used. For the KITTI-360 dataset, the training (6 sequences, 44178 frames), validation (2 sequences, 1115 frames) and testing (1 sequence, 2459 frames) splits from VSRD [4] are used. It is worth noting that, unlike VSRD, we are able to use all frames of the training set as our method is much faster.

b) Implementation: We used off-the-shelf MViT2-Huge [41] in the Detectron2 framework [42] trained on MS-COCO [43] as the 2D object detector and Metric3DV2-giant [9] for metric depth estimation. We use our pseudo-labels to train MonoDETR [19] monocular 3D object detector, using AdamW [44] optimiser with learning rate and weight decay equal to 0.0002 and 0.0001, respectively, while keeping other hyper-parameters as in [19]. The canonical focal length is equal to 500. Aggregation is done over 100 frames, the p -score threshold for stationary/moving classification is 0.0001, and the minimum threshold for d_{real} is 5 meters. The steepness parameter α in the Saturated Closeness Criterion is 10.

A. Results

a) KITTI-360.: The first evaluation and comparison with prior work is on KITTI-360 [39] as shown in table I. Our method shows outstanding results on both the Bird’s eye view (BEV) and 3D at 0.5 IoU as it **outperforms current state-of-the-art** weakly-supervised method VSRD [4], despite the fact *our method does not use any human labels*.

In the 0.3 IoU metric both for BEV and 3D, our method outperforms both WeakM3D [1] and Autolabels [2] by a significant margin and it achieves a competitive AP as VSRD [4]. We believe that this is likely caused by the detection failures, class ambiguities or that KITTI 2D bounding boxes are amodal as using consistent ground-truth 2D labels significantly helps VSRD.

b) Cross-dataset evaluation: Thanks to the proposed Canonical Object Space, it is possible to train on multiple merged datasets. We, therefore, combine both KITTI and KITTI-360 datasets training subsets, generate our pseudo-labels, train a single model and evaluate it on the KITTI validation subset (see table II). We show that generating pseudo-labels for two different datasets and then performing training on the joint significantly improves average precision both for 0.3 and 0.5 IoU on BEV and 3D. The gain comes from the additional amount of data present in the KITTI-360 dataset.

Method	Training supervision			3D Object detection accuracy				Labelling speed per frame
	LiDAR	Human Labels		AP _{BEV} /AP _{3D} @0.5		AP _{BEV} /AP _{3D} @0.3		
		Masks	3D boxes	Easy	Hard	Easy	Hard	
Fully-supervised methods								
MonoFlex [23]	yes*	✗	yes	50.82/43.11	41.78/34.43	69.70/67.07	59.86/57.26	-
MonoDETR [19]	yes*	✗	yes	47.21/41.01	36.05/30.38	63.07/60.49	54.04/50.03	-
Methods requiring some human annotations								
WeakM3D [1]	yes	yes	✗	8.10/2.96	2.96/2.01	29.89/21.25	24.01/15.34	80 ms
Autotlabels [2]	yes	yes	✗	20.18/4.69	14.33/2.79	48.16/12.92	37.34/9.94	6 sec
VSRD [4]	✗	yes	✗	29.07/21.77	22.83/16.46	58.40/50.86	50.61/43.45	15 min
Methods without human annotations								
Ours	✗	✗	✗	38.41/29.98	35.26/27.56	50.84/42.72	49.22/46.59	5 sec

TABLE I: Evaluation results of monocular 3D object (vehicle) detection on the KITTI-360 test set. * denotes that given data modality was not used by the method itself, but it was required in the annotation process to create human 3D box annotations.

Dataset for training	Labels	AP _{BEV} /AP _{3D} @0.5			AP _{BEV} /AP _{3D} @0.3		
		Easy	Moderate	Hard	Easy	Moderate	Hard
KITTI	pseudo	59.76/51.55	44.08/37.09	36.99/33.15	73.38/72.70	57.23/56.30	48.59/47.70
K360	pseudo	57.62/47.39	43.86/38.33	37.05/32.23	75.83/74.40	63.69/61.56	55.75/53.85
KITTI + K360	pseudo	62.28/53.04	46.38/40.79	42.38/35.10	79.70/78.48	65.85/63.97	57.41/55.46
KITTI	human	67.44/65.09	53.46/47.39	46.80/44.58	80.30/79.72	67.16/65.87	59.54/58.83

TABLE II: Monocular 3D object detection accuracy on the KITTI validation set, depending on which datasets/labels are used in training.

We also demonstrate the ability of our method to *work out-of-the-box in previously unseen camera setup* (see table II - row K360), where the model was trained using pseudo-labels on KITTI-360 but evaluated on in this case unseen KITTI dataset. We note that considering IoU 0.3, the accuracy of a model trained on KITTI-360 is actually even slightly higher than the model trained on the original domain (KITTI), which we contribute simply to the fact that KITTI-360 contains more training data.

Method	GT Ratio	AP _{BEV} /AP _{3D} @0.7		
		Easy	Moderate	Hard
VSRD [4]	0%	0.002/0.001	0.004/0.001	0.005/0.002
Ours		24.46/8.24	20.03/6.84	16.14/6.36
VSRD [4]	25%	31.72/21.76	22.32/15.43	18.86/12.55
Ours		39.99/32.64	30.92/25.06	26.47/20.35
VSRD [4]	50%	43.44/31.05	31.54/21.48	27.17/17.93
Ours		44.32/33.70	32.97/25.65	27.52/23.08
VSRD [4]	75%	42.58/32.95	31.08/24.68	27.19/21.38
Ours		43.32/34.11	32.48/25.68	27.39/23.05
MonoDETR [19]	100%	37.99/29.36	26.76/20.64	23.02/17.30

TABLE III: 3D object detection accuracy on KITTI validation set depending on the fraction of human labels used to fine-tune the model.

c) Semi-supervised: In this experiment, MonoDETR is trained jointly on KITTI and KITTI-360, while all labels are generated by our auto-labelling pipeline, as a pre-training step. Next, only a given fraction of human labels is used to fine-tune the model.

Firstly, as seen in table III, thanks to COS our method works out-of-the-box without any fine-tuning (0% human labels), unlike previous methods, showing there is no need to fine-tune using human labels while moving to different domains.



Fig. 7: Example 3D car detections of our model trained without using human annotations on both KITTI [8] and KITTI-360 [39].

Secondly, pre-training on a larger dataset auto-labelled by our method and then fine-tuning on the target domain significantly improves the average precision over simply training on the target domain from scratch. *With only 25% of the ground truth labels*, our method **outperforms** traditional fully-supervised detector trained from scratch with 100% of human labels, and the gap grows as more human labels are used. Lastly, our method significantly outperforms current state-of-the-art VSRD [4] by a large margin, showing that pre-training on larger datasets is a promising direction for further research.

B. Ablations

a) Canonical Object Space: As seen in table IV, disabling COS and training on both datasets jointly decreases the average precision of both BEV and 3D. It may be surprising that when training on both KITTI+K360, the model is not broken

Dataset for training	COS	AP _{BEV} /AP _{3D} @0.3		
		Easy	Moderate	Hard
KITTI	✗	80.30/79.72	67.16/65.87	59.54/58.83
KITTI+K360	✗	71.71/69.62	59.44/57.89	53.76/52.25
KITTI+K360	✓	82.07/81.25	67.14/66.16	62.47/61.02

TABLE IV: Canonical Object Space (COS) ablation on KITTI validation set under full supervision from human labels.

No. of frames	AP _{BEV} /AP _{3D} @0.5		
	Easy	Moderate	Hard
± 1	53.26/49.35	41.34/35.86	34.77/29.14
± 10	59.76/61.55	44.08/37.09	36.99/33.15
± 30	59.22/51.18	42.65/36.64	35.91/29.77

TABLE V: Number of frames used in the aggregation process ablation on KITTI validation set.

completely – we speculate that the network is able to learn to classify from which of the two datasets the image comes from and adjusts its outputs accordingly; such an approach obviously does not generalize well. Note that only in this ablation, we use human labels to eliminate any effects of pseudo-labels.

b) Number of frames used in aggregation: table V shows the ablation study on the number of frames used in the aggregation process. Perhaps surprisingly, aggregating over longer sequences does not yield better performance. The aggregation can recover from the error caused by Metric3D [3], [9] as in fig. 4. We speculate that the distant car poses a significant challenge for the detector itself, therefore creating precise 3D labels for such objects does not translate to better 3D detection accuracy.

α	AP _{BEV} /AP _{3D} @0.5		
	Easy	Moderate	Hard
1	53.02/48.09	41.29/34.92	34.48/28.66
5	55.14/50.83	42.46/36.59	35.92/29.85
10	56.56/48.90	41.32/35.00	34.53/28.76
15	55.78/51.86	42.48/36.63	35.72/29.81

TABLE VI: Steepness parameter α of the Saturated Closeness Criterion ablation on KITTI validation set.

c) Steepness parameter in Saturated Closeness Criterion:

In this ablation, we explore possible values for the steepness parameter α in the Saturated Closeness Criterion, which controls what pseudo-LIDAR points are discarded as outliers. As shown in table VI, α equal to 10 achieves the best performance.

V. CONCLUSION

A novel method for training monocular 3D detectors without domain-specific human annotations was presented. The method exploits temporal consistency in video sequences to automatically create 3D labels of objects (cars) and, as such, does not require human labels or additional sensors such as LiDAR. The method is able to compensate for camera focal length differences to significantly improve its scalability across

multiple datasets, and furthermore, it works out of the box in previously unseen camera setups.

The method is evaluated on two large-scale public datasets, where despite using no human labels, it outperforms prior work by a significant margin both for BEV and 3D when using the stricter 0.5 IoU evaluation. Last but not least, the method shows its versatility by also being a powerful pre-training method for fully-supervised monocular 3D detection, where the final accuracy increases by approximately 6 percent points over traditional object detector.

The main limitation is detecting objects far away, which is not primarily due to the auto-labelling procedure but due to the inherent limitation of the trained monocular detector to infer the distance of objects which are only a couple of pixels high.

REFERENCES

- [1] L. Peng, S. Yan, B. Wu, Z. Yang, X. He, and D. Cai, “Weakm3d: Towards weakly supervised monocular 3d object detection,” in *International Conference on Learning Representations*, 2022. 1, 6, 7
- [2] S. Zakharov, W. Kehl, A. Bhargava, and A. Gaidon, “Autolabeling 3d objects with differentiable rendering of sdf shape priors,” in *Proceedings of the IEEE/CVF Conference on Computer Vision and Pattern Recognition*, pp. 12224–12233, 2020. 1, 2, 6, 7
- [3] W. Yin, C. Zhang, H. Chen, Z. Cai, G. Yu, K. Wang, X. Chen, and C. Shen, “Metric3d: Towards zero-shot metric 3d prediction from a single image,” in *Proceedings of the IEEE/CVF International Conference on Computer Vision*, pp. 9043–9053, 2023. 1, 2, 3, 6, 8
- [4] Z. Liu, H. Sakuma, and M. Okutomi, “Vsr: Instance-aware volumetric silhouette rendering for weakly supervised 3d object detection,” in *Proceedings of the IEEE/CVF Conference on Computer Vision and Pattern Recognition*, pp. 17354–17363, 2024. 1, 2, 6, 7
- [5] R. Ranftl, K. Lasinger, D. Hafner, K. Schindler, and V. Koltun, “Towards robust monocular depth estimation: Mixing datasets for zero-shot cross-dataset transfer,” *IEEE transactions on pattern analysis and machine intelligence*, vol. 44, no. 3, pp. 1623–1637, 2020. 2
- [6] S. F. Bhat, R. Birkel, D. Wofk, P. Wonka, and M. Müller, “Zoedepth: Zero-shot transfer by combining relative and metric depth,” *arXiv preprint arXiv:2302.12288*, 2023. 2
- [7] L. Yang, B. Kang, Z. Huang, X. Xu, J. Feng, and H. Zhao, “Depth anything: Unleashing the power of large-scale unlabeled data,” in *Proceedings of the IEEE/CVF Conference on Computer Vision and Pattern Recognition*, pp. 10371–10381, 2024. 2
- [8] A. Geiger, P. Lenz, C. Stiller, and R. Urtasun, “Vision meets robotics: The kitti dataset,” *The International Journal of Robotics Research*, vol. 32, no. 11, pp. 1231–1237, 2013. 2, 6, 7
- [9] M. Hu, W. Yin, C. Zhang, Z. Cai, X. Long, H. Chen, K. Wang, G. Yu, C. Shen, and S. Shen, “Metric3d v2: A versatile monocular geometric foundation model for zero-shot metric depth and surface normal estimation,” *arXiv preprint arXiv:2404.15506*, 2024. 2, 6, 8
- [10] M. Oquab, T. Darcet, T. Moutakanni, H. Vo, M. Szafraniec, V. Khalidov, P. Fernandez, D. Haziza, F. Massa, A. El-Nouby, *et al.*, “Dinov2: Learning robust visual features without supervision,” *arXiv preprint arXiv:2304.07193*, 2023. 2
- [11] Z. Liu, H. Mao, C.-Y. Wu, C. Feichtenhofer, T. Darrell, and S. Xie, “A convnet for the 2020s,” in *Proceedings of the IEEE/CVF conference on computer vision and pattern recognition*, pp. 11976–11986, 2022. 2
- [12] R. Ranftl, A. Bochkovskiy, and V. Koltun, “Vision transformers for dense prediction,” in *Proceedings of the IEEE/CVF international conference on computer vision*, pp. 12179–12188, 2021. 2
- [13] J. M. Facil, B. Ummenhofer, H. Zhou, L. Montesano, T. Brox, and J. Civera, “Cam-convs: Camera-aware multi-scale convolutions for single-view depth,” in *Proceedings of the IEEE/CVF Conference on Computer Vision and Pattern Recognition*, pp. 11826–11835, 2019. 2
- [14] X. Weng and K. Kitani, “Monocular 3d object detection with pseudo-lidar point cloud,” in *Proceedings of the IEEE/CVF International Conference on Computer Vision Workshops*, pp. 0–0, 2019. 2

- [15] Y. Wang, W.-L. Chao, D. Garg, B. Hariharan, M. Campbell, and K. Q. Weinberger, "Pseudo-lidar from visual depth estimation: Bridging the gap in 3d object detection for autonomous driving," in *Proceedings of the IEEE/CVF conference on computer vision and pattern recognition*, pp. 8445–8453, 2019. 2
- [16] X. Ma, Z. Wang, H. Li, P. Zhang, W. Ouyang, and X. Fan, "Accurate monocular 3d object detection via color-embedded 3d reconstruction for autonomous driving," in *Proceedings of the IEEE/CVF international conference on computer vision*, pp. 6851–6860, 2019. 2
- [17] Z. Liu, Z. Wu, and R. Tóth, "Smoke: Single-stage monocular 3d object detection via keypoint estimation," in *Proceedings of the IEEE/CVF conference on computer vision and pattern recognition workshops*, pp. 996–997, 2020. 2
- [18] K.-C. Huang, T.-H. Wu, H.-T. Su, and W. H. Hsu, "Monodtr: Monocular 3d object detection with depth-aware transformer," in *Proceedings of the IEEE/CVF conference on computer vision and pattern recognition*, pp. 4012–4021, 2022. 2
- [19] R. Zhang, H. Qiu, T. Wang, Z. Guo, Z. Cui, Y. Qiao, H. Li, and P. Gao, "Monodetr: Depth-guided transformer for monocular 3d object detection," in *Proceedings of the IEEE/CVF International Conference on Computer Vision*, pp. 9155–9166, 2023. 2, 6, 7
- [20] A. Vaswani, "Attention is all you need," *Advances in Neural Information Processing Systems*, 2017. 2
- [21] X. He, F. Yang, K. Yang, J. Lin, H. Fu, M. Wang, J. Yuan, and Z. Li, "Ssd-monodetr: Supervised scale-aware deformable transformer for monocular 3d object detection," *IEEE Transactions on Intelligent Vehicles*, 2023. 2
- [22] Y. Zhou, H. Zhu, Q. Liu, S. Chang, and M. Guo, "Monoatt: Online monocular 3d object detection with adaptive token transformer," in *Proceedings of the IEEE/CVF Conference on Computer Vision and Pattern Recognition*, pp. 17493–17503, 2023. 2
- [23] Y. Zhang, J. Lu, and J. Zhou, "Objects are different: Flexible monocular 3d object detection," in *Proceedings of the IEEE/CVF Conference on Computer Vision and Pattern Recognition*, pp. 3289–3298, 2021. 2, 7
- [24] L. Yan, P. Yan, S. Xiong, X. Xiang, and Y. Tan, "Monocod: Monocular 3d object detection with complementary depths," in *Proceedings of the IEEE/CVF Conference on Computer Vision and Pattern Recognition*, pp. 10248–10257, 2024. 2
- [25] Z. Qin, J. Wang, and Y. Lu, "Weakly supervised 3d object detection from point clouds," in *Proceedings of the 28th ACM International Conference on Multimedia*, pp. 4144–4152, 2020. 2
- [26] J. J. Park, P. Florence, J. Straub, R. Newcombe, and S. Lovegrove, "DeepSDF: Learning continuous signed distance functions for shape representation," in *Proceedings of the IEEE/CVF conference on computer vision and pattern recognition*, pp. 165–174, 2019. 2
- [27] Q. Meng, W. Wang, T. Zhou, J. Shen, L. Van Gool, and D. Dai, "Weakly supervised 3d object detection from lidar point cloud," in *ECCV*, 2020. 2
- [28] Q. Meng, W. Wang, T. Zhou, J. Shen, Y. Jia, and L. Van Gool, "Towards a weakly supervised framework for 3d point cloud object detection and annotation," *IEEE Transactions on Pattern Analysis and Machine Intelligence*, vol. 44, no. 8, pp. 4454–4468, 2021. 2
- [29] R. McCraith, E. Insafutdinov, L. Neumann, and A. Vedaldi, "Lifting 2D object locations to 3D by discounting LiDAR outliers across objects and views," in *2022 International Conference on Robotics and Automation (ICRA)*, pp. 2411–2418, 2022. 2, 3, 6
- [30] K. He, G. Gkioxari, P. Dollár, and R. Girshick, "Mask r-cnn," in *Proceedings of the IEEE international conference on computer vision*, pp. 2961–2969, 2017. 2
- [31] J. Skvrna and L. Neumann, "TCC-Det: Temporarily consistent cues for weakly-supervised 3D detection," in *European Conference on Computer Vision*, pp. 129–145, Springer, 2024. 2, 5, 6
- [32] K.-C. Huang, Y.-H. Tsai, and M.-H. Yang, "Weakly supervised 3d object detection via multi-level visual guidance," in *ECCV*, 2024. 2
- [33] M. Goldstein and A. Dengel, "Histogram-based outlier score (hbos): A fast unsupervised anomaly detection algorithm," *KI-2012: poster and demo track*, vol. 1, pp. 59–63, 2012. 3
- [34] Q.-Y. Zhou, J. Park, and V. Koltun, "Open3D: A modern library for 3D data processing," *arXiv:1801.09847*, 2018. 3
- [35] L. McInnes, J. Healy, S. Astels, *et al.*, "hdbscan: Hierarchical density based clustering," *J. Open Source Softw.*, vol. 2, no. 11, p. 205, 2017. 3
- [36] M. Ester, H.-P. Kriegel, J. Sander, X. Xu, *et al.*, "A density-based algorithm for discovering clusters in large spatial databases with noise," in *kdd*, vol. 96, pp. 226–231, 1996. 3
- [37] X. Zhang, W. Xu, C. Dong, and J. M. Dolan, "Efficient l-shape fitting for vehicle detection using laser scanners," in *2017 IEEE Intelligent Vehicles Symposium (IV)*, pp. 54–59, IEEE, 2017. 4, 5
- [38] P. Sun, H. Kretzschmar, X. Dotiwalla, A. Chouard, V. Patnaik, P. Tsui, J. Guo, Y. Zhou, Y. Chai, B. Caine, V. Vasudevan, W. Han, J. Ngiam, H. Zhao, A. Timofeev, S. Ettinger, M. Krivokon, A. Gao, A. Joshi, Y. Zhang, J. Shlens, Z. Chen, and D. Anguelov, "Scalability in perception for autonomous driving: Waymo open dataset," in *Proceedings of the IEEE/CVF Conference on Computer Vision and Pattern Recognition (CVPR)*, June 2020. 6
- [39] Y. Liao, J. Xie, and A. Geiger, "Kitti-360: A novel dataset and benchmarks for urban scene understanding in 2d and 3d," *IEEE Transactions on Pattern Analysis and Machine Intelligence*, vol. 45, no. 3, pp. 3292–3310, 2022. 6, 7
- [40] Y. Wei, S. Su, J. Lu, and J. Zhou, "Fgr: Frustum-aware geometric reasoning for weakly supervised 3d vehicle detection," in *2021 IEEE International Conference on Robotics and Automation (ICRA)*, pp. 4348–4354, IEEE, 2021. 6
- [41] Y. Li, C.-Y. Wu, H. Fan, K. Mangalam, B. Xiong, J. Malik, and C. Feichtenhofer, "Mvitv2: Improved multiscale vision transformers for classification and detection," in *Proceedings of the IEEE/CVF conference on computer vision and pattern recognition*, pp. 4804–4814, 2022. 6
- [42] Y. Wu, A. Kirillov, F. Massa, W.-Y. Lo, and R. Girshick, "Detectron2," <https://github.com/facebookresearch/detectron2>, 2019. 6
- [43] T.-Y. Lin, M. Maire, S. Belongie, J. Hays, P. Perona, D. Ramanan, P. Dollár, and C. L. Zitnick, "Microsoft COCO: Common objects in context," in *Computer Vision—ECCV 2014: 13th European Conference, Zurich, Switzerland, September 6–12, 2014, Proceedings, Part V 13*, pp. 740–755, Springer, 2014. 6
- [44] I. Loshchilov, "Decoupled weight decay regularization," *arXiv preprint arXiv:1711.05101*, 2017. 6